RSC Advances

PAPER

View Article Online
View Journal | View Issue

Cite this: *RSC Adv.*, 2014, **4**, 20102

Transport properties of $APdCu(Se_2)(Se_3)$ (A = K and Rb): new quaternary copper palladium polyselenides

Sikander Azam*[a] and A. H. Reshak[ab]

The electronic structure, effective mass, optical properties and electrical transport coefficients of $APdCu(Se_2)(Se_3)$ (where A = K and Rb), a new quaternary copper palladium polyselenide, were investigated using a density functional theory calculation within a generalized gradient approximation (GGA) plus the Hubbard term (U) (GGA + U). The electronic band structure shows that the calculated compounds have a direct band gap. From the partial density of states we found that, at an energy of −5.0 eV: (1) the Pd-s state strongly hybridizes with the Se-p state; (2) near the Fermi level the Se-p state hybridizes with the Cu-p state; and (3) at the lower conduction band the Pd-s state forms a strong hybridization with the Cu-s state. The investigation of electronic charge density shows that the Pd–Se and Cu–Se atoms form weak covalent bonds and have strong ionicity, whereas the K/Pd atoms exhibit pure ionic bonding. We also calculated the dielectric function, refractive index, extinction coefficient, absorption coefficient and reflectivity of the compounds. The calculated transport coefficients show the anisotropic nature of the compounds, in agreement with their electronic states. The transport properties reveal stronger carrier transport along the Cu-p/d and Pd-d orbitals, indicating that these orbitals are mainly responsible for the electrical transport. The maximum power factor values of the $KPdCu(Se_2)(Se_3)$ ($RbPdCu(Se_2)(Se_3)$) compounds as a function of relaxation time reach 2.2 (1.8) × 10^{11}, 4.4 (3.5) × 10^{11} and 1.3 (1.4) × 10^{11} within P^{xx}, P^{yy} and P^{zz} components, respectively.

Received 20th March 2014
Accepted 7th April 2014

DOI: 10.1039/c4ra02465f

www.rsc.org/advances

1. Introduction

Chalcogenide compounds have a very diverse and interesting structural chemistry and show useful physical and chemical properties that may be applicable to modern technologies.[1] The synthesis of binary and ternary chalcogenides has been extensively studied using high temperature solid state, intermediate temperature flux, and low temperature solvothermal techniques. However, comparatively little is known about quaternary chalcogenides, which may also demonstrate interesting properties.[2–5] The synthesis of novel quaternary chalcogenides has recently become an active area of research in solid state chemistry.[2,4,5] Most known quaternary chalcogenides are made using the molten alkali metal polychalcogenide flux technique, although low temperature solvo(hydro)thermal reactions have produced a limited number of quaternary chalcogenides.[6]

Pd-holding compounds have received much consideration as a result of the catalytic functions of the metal and its capacity to form polychalcogenide complexes in solution. Several ternary Pd polychalcogenides have now been isolated and structurally characterized. These include: $(Ph_4P)_2[Pd(Se_4)_2]$, with distinct $[Pd(Se_4)_2]^{2-}$ anions in which each Pd^{2+} is coordinated by two chelating $(Se_4)^{2-}$ ligands;[7] $\{(CH_3)N(CH_2CH_2)_3N\}_2[Pd(Se_6)_2]$ and $(enH)_2[Pd(Se_5)_2]$, which feature sheet-like, two-dimensional Pd polyselenide anionic frameworks;[8] $Rb_2[Pd(Se_4)_2]Se_8$, encompassing the sheet-like polyanion $[Pd(Se_4)_2]^{2-}$ with intercalated crown-like Se_8 eight-membered rings;[9] and $K_4[Pd(Se_4)2][Pd(Se_6)_2]$ (= K_2PdSe_{10}) and $Cs_2[Pd(Se_4)_2]$ (= Cs_2PdSe_8) with three-dimensional structures assembled from two interpenetrating $[Pd(Se_x)_2]^{2-}$ structures ($x = 4$ and 6 for the K^+ saline, $x = 4$ and 4 for the Cs^+ salt).[10,11]

In the system A–M–M′–Q (A = alkali steel, M = assembly I element, M′ = assembly VIII steel, Q = chalcogen), only a few Fe compounds with the crystal formula $AMFeQ_2$ (A = Li, Na, K, Cs; M = Cu, Ag; Q = S, Se, Te) are known.[12–16] In 2003, Chen *et al.*[17] reported the groundwork, crystal organization, and optical and thermal properties of two innovative mixtures: $APdCu(Se_2)(Se_3)$ (A = K and Rb), which were the first quaternary copper palladium polychalcogenides obtained by solvothermal procedures utilizing ethylenediamine (en) as the reaction medium. The target of the present study was the evaluation of $APdCu(Se_2)(Se_3)$ (A = K and Rb). We calculated the thermoelectric properties of the compounds, which have not previously been reported.

This paper aims provide a systematic study of the electronic band structure and optical and thermoelectric properties of

[a]*New Technologies – Research Centre, University of West Bohemia, Univerzitni 8, 306 14 Pilsen, Czech Republic. E-mail: sikander.physicst@gmail.com*

[b]*Center of Excellence Geopolymer and Green Technology, School of Material Engineering, University Malaysia Perlis, 01007 Kangar, Perlis, Malaysia*

$APdCu(Se_2)(Se_3)$ (A = K and Rb) using density functional theory (DFT) + U calculations. The generalized gradient approximation (GGA) + U exchange potential approximation was used to calculate accurately the electronic band structure and optical and thermoelectric properties of $APdCu(Se_2)(Se_3)$ (A = K and Rb) as the DFT + U scheme for solids has been shown to give better band gaps than semi-local DFT methods.[18,19]

The optical properties help us to obtain a deep insight into the structure of $APdCu(Se_2)(Se_3)$ (A = K and Rb). The electrical transport parameters (conductivity, Seebeck coefficient, power factor) for the compound system were obtained theoretically based on the DFT calculations and the rigid band approach.

We briefly describe the computational method used in this study and then present and discuss the most relevant results obtained for the electronic, optical and thermoelectric properties of $APdCu(Se_2)(Se_3)$ (A = K and Rb).

2. Methodology

It was recently reported that the local density approximation (LDA) and GGA schemes are insufficient to describe correctly the electronic structure of transition metal oxides.[20] The GGA + U (where U is the Hubbard term) method was therefore applied here to account for on-site correlation at the transition metal sites. The GGA + U method, which accounts for an orbital dependence of the Coulomb-exchange interaction, was used. The crystal structure of the new quaternary copper palladium polyselenides with monoclinic symmetry was determined by Chen *et al.*[17] The unit cell with the formula $APdCu(Se_2)(Se_3)$ (A = K and Rb) was modeled for the pure phase property calculation simulations, *i.e.* the electronic states and transport parameter calculation. The unit cell crystal structures for both compounds are illustrated in Fig. 1. Calculations with the full potential linear augmented plane wave method based on DFT[21,22] theory were performed using the Wien2k package.[23] The exchange and correlation were computed within GGA + U.[24]

The ground state properties of the resulting optimized structures were computed by performing self-consistent interactions until the iterative convergence of energy and charge to values of $<10^{-5}$ R_y and $<10^{-4}$ C, respectively. We calculated the bond lengths and angles, which show good agreement with the experimental data[17] (Tables 1 and 2). We used the parameter $R_{MT}K_{MAX} = 7$ (where R_{MT} is the smallest of the muffin-tin radii and K_{MAX} is the plane wave cutoff) to control the size of the basis set for the wave functions. The electronic band structure, total and partial density of states and the linear optical susceptibilities were calculated using summation over 1000 k-points within the IBZ. The Monkhorst–pack grid 11 × 10 × 8 was used for k-point sampling in the electronic state calculation. The high symmetry k-points in the Brillouin zone (BZ) within our calculated band structure are Z → B → G → Y → G → Z. To initiate the calculations, we used the experimental values for lattice parameters from Chen *et al.*[17] The atomic positions are fully optimized by minimizing the forces acting on each atom. The optical properties of matter can be described by the dielectric function $\varepsilon(\omega)$. In the limit of linear optics, neglecting electron polarization effects and within the frame of random

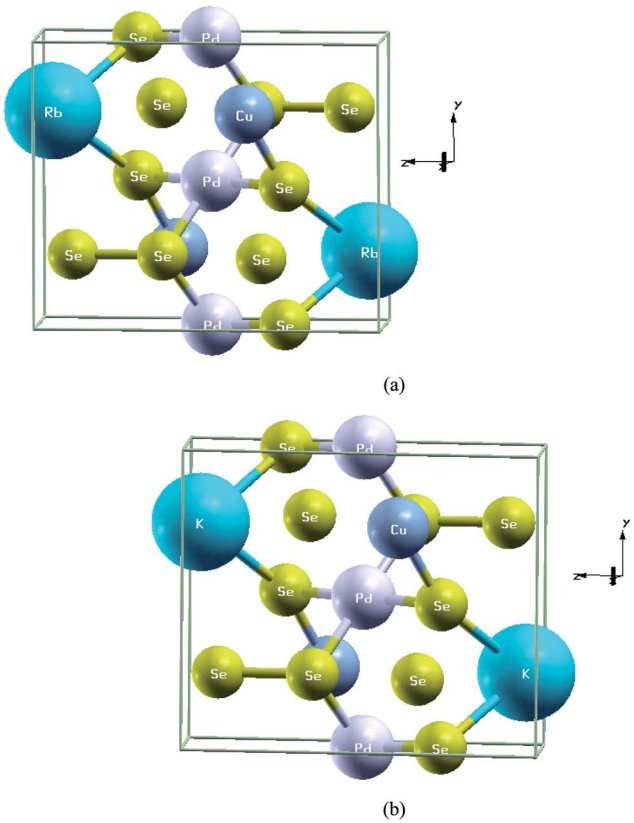

Fig. 1 Unit cell structures. (a) $RbPdCu(Se_2)(Se_3)$ unit cell structure; and (b) $KPdCu(Se_2)(Se_3)$ unit cell structure.

phase approximation, the expression for the imaginary part $\varepsilon_2(\omega)$ of the dielectric function is calculated from the momentum matrix elements between the occupied and unoccupied wave functions. The real part $\varepsilon_1(\omega)$ of the dielectric function is evaluated from the imaginary part $\varepsilon_2(\omega)$ by the Kramers–Kroning transformation. The other optical constants, such as the reflective index, extinction coefficient, reflectivity and energy-loss spectrum can be obtained from $\varepsilon_1(\omega)$ and $\varepsilon_2(\omega)$.

The electrical transport coefficients were calculated within the framework of semi-classical Boltzmann theory and the rigid band approach by analyzing the band structure from the DFT calculations.[25,26] The transport distribution function to conductivity within the rigid band approach is based on the following tensor:

$$\sigma_{\alpha\beta}(\varepsilon) = \frac{1}{N}\sum_{i,k}\sigma_{\alpha\beta}(i,k)(\varepsilon - \varepsilon_{i,k}) \quad (1)$$

where $1/N$ accounts for the normalization of the sum so it is the integral in the limit where the number of grid points becomes dense, $\varepsilon_{i,k}$ is the electron band energy for band i at the Brillouin k point and $\sigma_{\alpha\beta}(i, k)$ is the k-dependent conductivity tensor expressed as

$$\sigma_{\alpha\beta}(i, k) = e^2\tau_{i,k}\nu_\alpha(i, k)\nu_\beta(i, k)\tau \quad (2)$$

where the $\nu_\alpha(i, k)$, $\nu_\beta(i, k)$, τ are the components of the band velocities and the relaxation time, respectively. In the band velocity expression, $\nu_\alpha(i, k)$ i denotes the bands, k denotes the

Table 1 Bond lengths in angstroms

$KPdCu(Se_2)(Se_3)$	Optimized	Experimental	$RbPdCu(Se_2)(Se_3)$	Optimized	Experimental
Cu–Se4	2.3657	2.369(1)	Pd–Se4	2.4760	2.454(2)
Cu–Se1	2.4571	2.467(2)	Cu–Se4	2.3598	2.362(2)
Cu–Se3	2.3765	2.411(2)	Cu–Se3	2.3748	2.411(4)
K–Se3	3.4387	3.458(4)	Cu–Se1	2.4583	2.479(3)
Pd–Se1	2.4723	2.4515(9)	Se1–Se2	2.3794	2.337(4)
Pd–Se4	2.4758	2.458(1)	Se3–Se4	2.4441	2.383(2)
Se1–Se2	2.3851	2.338(2)	Rb–Se2	3.4140	3.407(3)
K–Se4	3.4121	3.423(3)	Rb–Se2	3.6681	3.420(3)
K–Se2	3.6625	3.6656(7)	Rb–Se2	3.6681	3.6702(7)
K–Se2	3.3297	3.349(4)	Rb–Se3	3.5010	3.524(4)
K–Se2	3.2941	3.299(3)	Pd–Se1	2.4746	2.455(2)
Se3–Se4	2.4484	2.390(1)	Rb–Se4	3.6209	3.525(3)
K–Se4	3.5072	3.541(3)	Rb–Se4	3.5089	3.656(3)

Table 2 Bond angles in degrees

$KPdCu(Se_2)(Se_3)$	Experimental	Optimized	$RbPdCu(Se_2)(Se_3)$	Experimental	Optimized
Se(1)–Pd–Se(4)	87.20(4)	87.22	Se(4)–Pd–Se(1)	87.55(7)	87.47
Se(1)–Pd–Se(4)	92.80(4)	92.78	Se(4)–Pd–Se(1)	92.45(7)	92.53
Se(1)–Pd–Se(1)	180	180	Se(1)–Pd–Se(1)	180	180
Se(4)–Pd–Se(4)	180	180	Se(4)–Pd–Se(4)	180	180
Se(3)–Cu–Se(1)	85.19(7)	85.48	Se(3)–Cu–Se(1)	84.6(1)	85.15
Se(4)–Cu–Se(4)	108.08(8)	106.77	Se(4)–Cu–Se(4)	107.8(1)	106.16
Se(4)–Cu–Se(1)	112.06(6)	111.11	Se(4)–Cu–Se(1)	114.2(1)	113.60
Se(4)–Cu–Se(3)	118.77(5)	120.15	Se(4)–Cu–Se(3)	117.4(1)	118.69
Se(4)–Se(3)–Se(4)	91.78(6)	90.26	Se(4)–Se(3)–Se(4)	92.8(1)	91.24
Se(3)–Se(4)–Pd	107.53(5)	106.20	Se(3)–Se(4)–Pd	107.74(9)	106.21
Se(2)–Se(1)–Pd	111.05(4)	109.65	Se(2)–Se(1)–Pd	110.73(8)	109.25
Pd–Se(1)–Pd	95.67(5)	94.60			

wave vector and α denotes the direction. The transport coefficients can then be determined by integrating the tensor within eqn (1) as a function of temperature as:

$$\sigma_{\alpha\beta}(T,\mu) = \frac{1}{\Omega}\int \sigma_{\alpha\beta}(\varepsilon)\left[-\frac{\partial f_\mu(T,E)}{\partial \varepsilon}\right]\mathrm{d}\varepsilon \quad (3)$$

where f is the Fermi distribution function, T is absolute temperature, μ is the chemical potential, ε is the energy and Ω is the volume. In the rigid band approach, the bands and $\sigma(\varepsilon)$ are fixed as only one band structure assessment is required.[27] The amount of carriers can be altered by varying the chemical potential μ. The thermal properties can be calculated from the band structure results except for the relaxation time. Theoretically, the relaxation time period is correlated with the crystal structure, temperature, doping content, microstructure and texture of specific materials.[28]

In general, the value of τ_e is determined by the ratio of the carrier energy $\varepsilon_{i,k}$ and the attained vibrational energy of atoms. The carrier power, $\varepsilon_{i,k}$ is dependent on the power catalogue i and the wave vector k, and the attained vibrational power of atoms is of the order of magnitude of $K_\beta T$. Much analytical research is needed to elucidate the scattering means and to determine the approximate value of τ_e for specific materials. Regardless of this, the relaxation time τ_e has been broadly measured as a constant and the carrier scattering has been assumed to be independent of the vector direction and temperature for the approximation of the real scattering means for convenience of calculation.[29,30]

Using the constant relaxation time approximation, the Seebeck coefficient can be determined by:

$$\alpha = \pm\frac{1}{eT}\left[E_F - \int_0^\infty g(E)\tau_e E^2 \frac{\mathrm{d}f_0(E)}{\mathrm{d}E}\Big/\int_0^\infty g(E)\tau_e E\frac{\mathrm{d}f_0(E)}{\mathrm{d}E}\right] \quad (4)$$

where e, E_F, $g(E)$ and τ_e are the electron charge, the Fermi level, the density of state and the relaxation time, respectively.[31] The Fermi level (E_F) and the density of state $g(E)$ as a function of E can be obtained from the calculated DFT results and the relaxation time τ_e is treated as roughly constant, therefore the Seebeck coefficient as a function of temperature T can be determined. The BoltzTraP program was used for the assessment of the k-dependent conductivity tensor. The BoltzTraP program relies on a smoothed Fourier interpolation to obtain an analytical expression of the bands.[32] The initial k mesh was interpolated up to a mesh five times denser than the original.

3. Results and discussion

3.1. Electronic structure

The GGA method is insufficient to describe systems in which the d-electrons are well localized and in which the spin orbital

interactions cannot be neglected, particularly their electronic properties. However, the GGA + *U* approach has been suggested to describe these systems. In this approach, the Hubbard term (*U*), which describes the d–d or f–f orbital interaction, is added to the GGA energy. This method has proved to be effective for describing strongly correlated systems.

We noticed that the band structures of the spin-up states are similar to those of the spin-down states. The electronic band structures of the monoclinic symmetry $KPdCu(Se_2)(Se_3)$ and $RbPdCu(Se_2)(Se_3)$ compounds were calculated and the calculated band structure profiles using the GGA + *U* approach are shown in Fig. 2. The electronic band dispersion curves are shown in addition to some high symmetry directions of the BZ for $KPdCu(Se_2)(Se_3)$ and $RbPdCu(Se_2)(Se_3)$ compounds. We will only consider the consequences of EV-GGA due to its improved band gap. The valence band maximum (VBM) and the conduction band minimum (CBM) are positioned at the *Y* point of BZ, resulting in a direct energy band gap of about 1.258/1.275 for $KPdCu(Se_2)(Se_3)$/$RbPdCu(Se_2)(Se_3)$. The calculated electronic structure of $KPdCu(Se_2)(Se_3)$ and $RbPdCu(Se_2)(Se_3)$ verifies that the investigated compounds are narrow gap semiconductors. To determine the nature of the electronic band structures, we calculated the total (TDOS) and partial (PDOS) density of states (DOS) for both compounds. A study of the DOS using the GGA + *U* approximation in both the spin-up and spin-down states shows that there is no remarkable difference between the two states (Fig. 3). Fig. 3 shows that there are three distinct structures separated by gaps. The first structure encountered in the TDOS (starting from the lower energies) consists entirely of K-p, Se-s and Rb-d states. These peaks are centered at about −14.0 to −10.0 eV for both compounds. The next structure, between −5.0 and 0.0 eV for both compounds, consists of the Pd-s/p, Cd-p/d and Se-p states. The conduction bands consist of Pd-s, Cu-s, Se-d, K-s

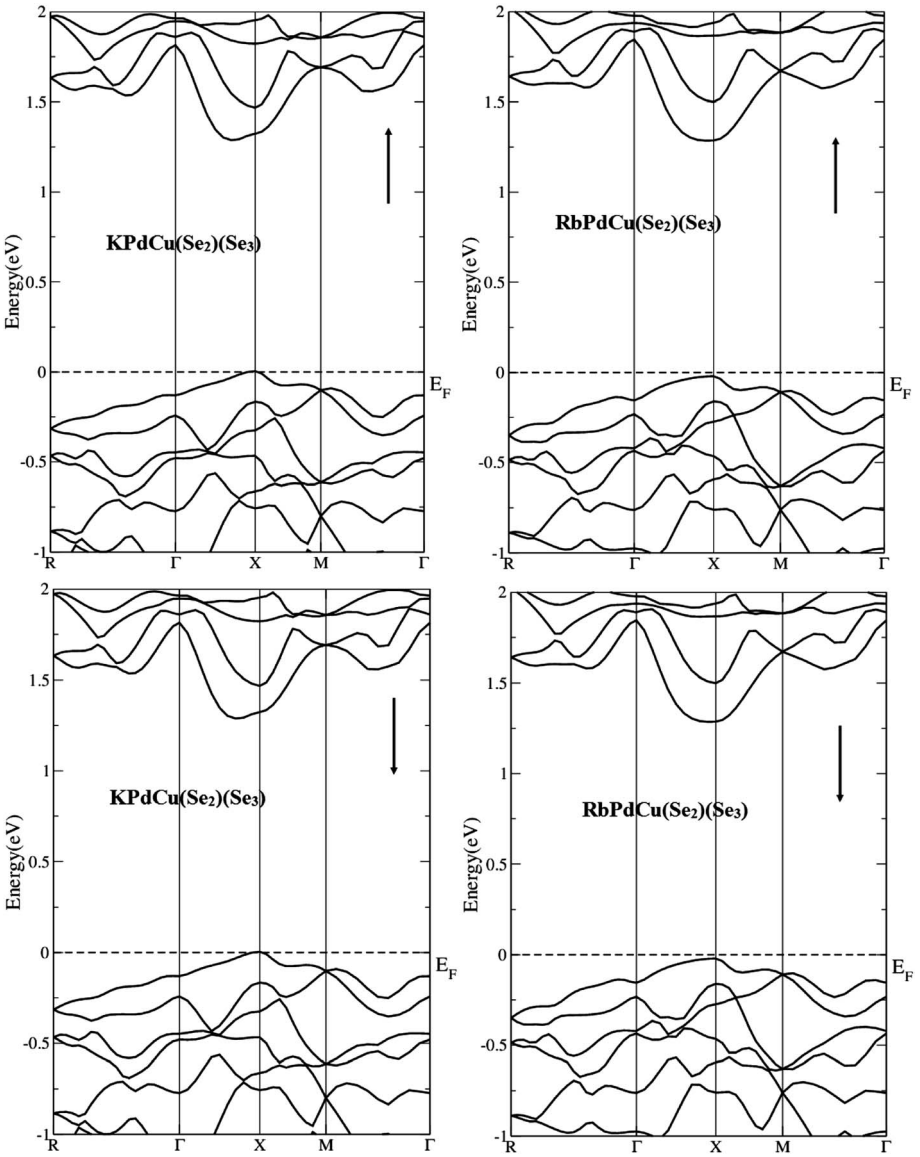

Fig. 2 Calculated band structures.

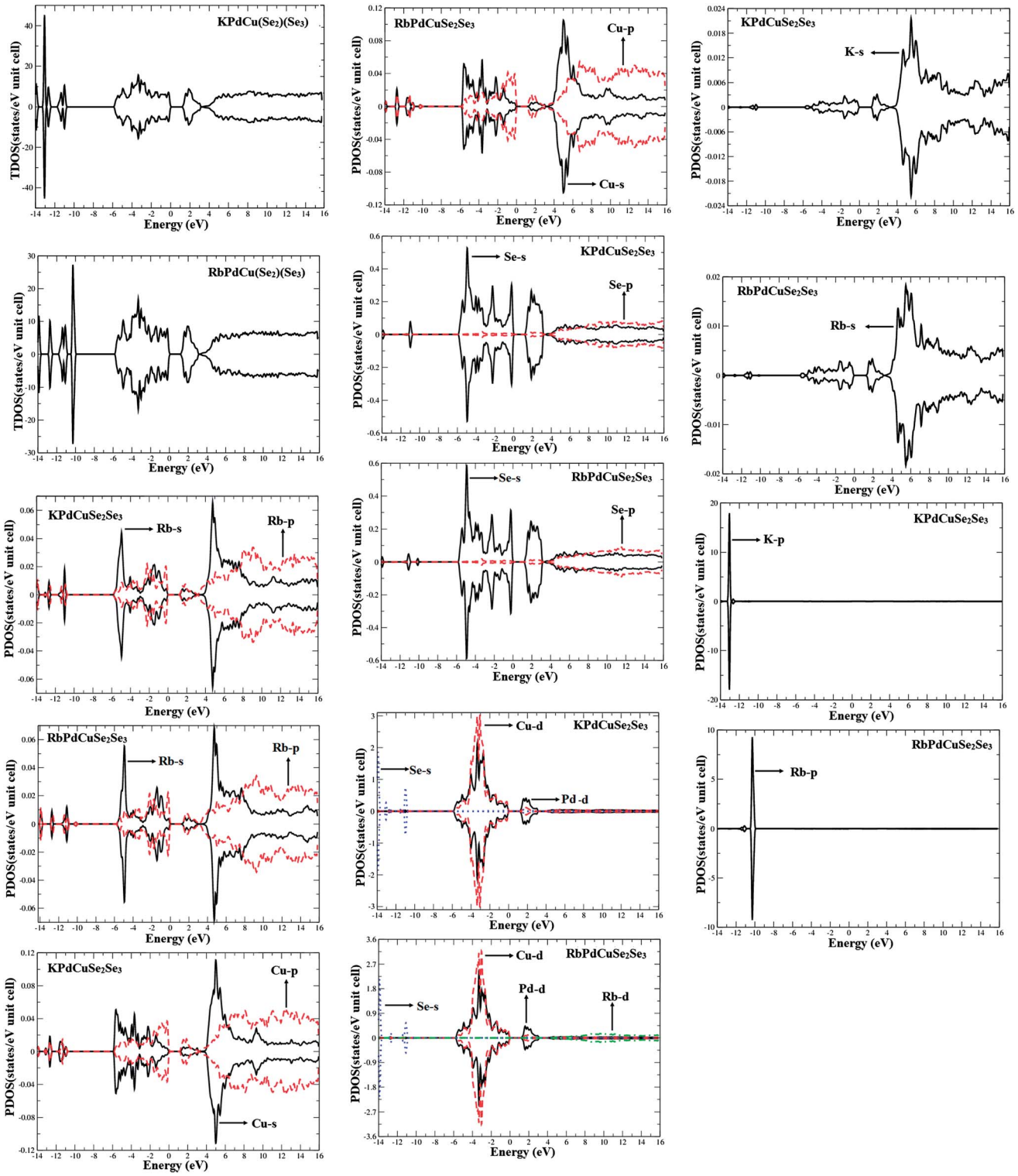

Fig. 3 Calculated total and partial densities of states (states per eV unit cell).

and Rb-d states. From the PDOS, we also concluded that at an energy of −5.0 eV, the Pd-s state forms a strong hybridization with the Se-p state. Near the Fermi level, the Se-p state hybridizes with the Cu-p state and at the low conduction band the Pd-s state strongly hybridizes with the Cu-s state.

3.2. Electron charge density

To establish a quantitative estimation for the type of bonding present in a particular molecule, it is necessary to have a measure of the extent of charge transfer present in the molecule relative to the charge distributions of the separated atoms. To

calculate the type of bonding in both the investigated compounds, we evaluated the atomic charge distributions using the FPLAPW method based on the DFT. The electron density contours give another approach to investigating the bonding interactions in solid materials and the changes in bonding which consequently lead to changes in the DOS.

The valence electronic charge density spectra are shown in Fig. 4 along the (110) crystallographic plane to help to understand the distribution of the total electronic charge density maps of the $KPdCu(Se_2)(Se_3)$ and $KPdCu(Se_2)(Se_3)$ compounds. The crystallographic planes show that there is both ionic and partial covalent bonding between the K, Rb, Pd, Cu and Se atoms depending on the Pauling electronegativity difference, *i.e.* the higher the associated electronegativity number, the more an element or compound attracts electrons towards it. The electronegativity of the K atom is (0.82), and the values for the other atoms are: Rb (0.79), Pd (2.20), Cu (1.90) and Se (2.55). The atoms Pd–Se and Cu–Se form weak covalent bonds and have strong ionicity, while the K/Pd atoms show pure ionic bonding. From these contour plots it can be seen that most of the Pd and Cu electronic charge is transferred to the Se atom. This can easily be seen by the color charge density scale, where blue (+1.0000) corresponds to the maximum charge accumulating site. The charge density along Pd and Se is pronounced. It is clear that when we replace K by Rb, the charge density decreases. As is clear from Fig. 4a, the charge density around Rb and Se is greater in $KPdCu(Se_2)(Se_3)$ than in $RbPdCu(Se_2)(Se_3)$.

3.3. Effective mass

We calculated the effective mass of electrons (m_e^*) from the electronic band structure. As we were interested in the energy bands around the Fermi level (E_F), we enlarged the band structure near E_F to show the bands which govern the energy band gap, *i.e.* the CBM and VBM. The values for the effective mass of electrons (m_e^*) were anticipated from the curvature of the conduction band minimum, band 125 for $KPdCu(Se_2)(Se_3)$ and band 135 for $RbPdCu(Se_2)(Se_3)$; these bands are highlighted in different colors (Fig. 2e and f). The diagonal elements of the effective mass tensor, m_e, for the electrons in the conduction band are calculated in the $\Gamma \rightarrow \Gamma$ direction in k space using the following well-known relation:

$$\frac{1}{m_e^*} = \frac{1\partial^2 E(k)}{\hbar^2 \partial k^2} \tag{5}$$

The effective mass of the electron is determined by fitting the electronic band structure to a parabolic function [eqn (5)] in the first BZ using the GGA + U approach. The effective mass of the electron for the (symmetry) is obtained from the curvature of the conduction band at the point Γ–Γ. The calculated effective mass ratios of the electron (m_e^*/m_e) for $KPdCu(Se_2)(Se_3)$ and $RbPdCu(Se_2)(Se_3)$ in the $\Gamma \rightarrow \Gamma$ direction are 0.0332 and 0.0225, respectively. The calculated value for $KPdCu(Se_2)(Se_3)$ is larger than that for $RbPdCu(Se_2)(Se_3)$. This is attributed to the fact that the parabolic curvature of $RbPdCu(Se_2)(Se_3)$ is greater than that of $KPdCu(Se_2)(Se_3)$ because the effective electron mass is inversely proportional to the curvature. We also calculated the effective mass of the heavy holes (the maximum valence band) and the light holes (the second maximum valence band) for $KPdCu(Se_2)(Se_3)$ and $RbPdCu(Se_2)(Se_3)$ from bands (134 and 133) and (124 and 123), respectively. The calculated values of the heavy holes and light holes for $KPdCu(Se_2)(Se_3)$ are 0.1350 and 0.1858 and for $RbPdCu(Se_2)(Se_3)$ 0.0202 and 0.0198, respectively.

3.4. Optical properties

The optical response functions of solids are often described by the complex dielectric function $\varepsilon(\omega) = \varepsilon_1(\omega) + i\varepsilon_2(\omega)$ or by the complex refractive index $N(\omega) = n(\omega) + ik(\omega)$.

$$\varepsilon_1(\omega) = n^2 - k^2 \tag{6}$$

$$\varepsilon_2(\omega) = 2nk \tag{7}$$

In determining the interaction between light and a solid, an adiabatic approximation and single-electron approximation are generally used. As the transition frequencies both within-band and between bands are much larger than the phonon frequency in the calculation of electronic structure and the method used is a single-electron approximation, phonon participation in the indirect transition process can be ignored and only electronic excitation considered. According to the definitions of the direct transition probabilities and the Kramers–Kronig dispersion relations, the imaginary and the real parts of the dielectric function, absorption coefficient, reflectivity and complex optical conductivity[33–35] can be deduced using:

$$\varepsilon_2(\omega) - = \frac{\pi e^2}{\varepsilon_0 m^2 \omega^2} \sum_{V,C} \left\{ \int_{BZ} \frac{2dk}{(2\pi)^2} \left| a \times M_{V,C} \right|^2 \delta[E_C(k) - E_V(k) - \hbar\omega] \right\} \tag{8}$$

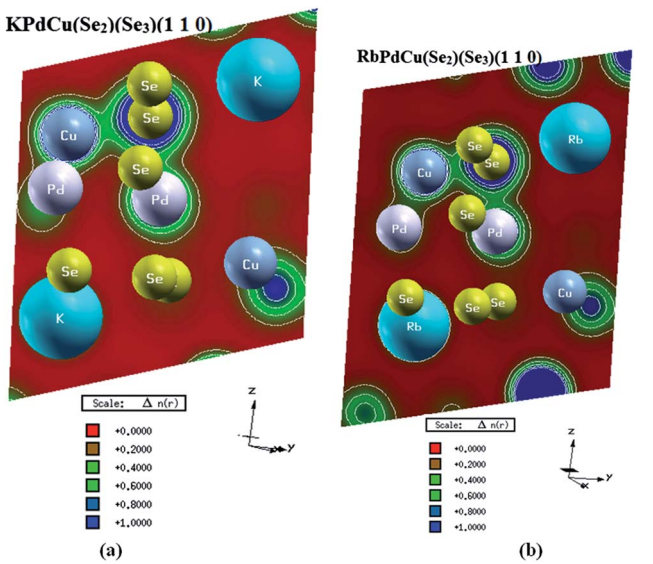

Fig. 4 Electronic charge density contours.

$$\varepsilon_1(\omega) = 1 + \frac{2e}{\varepsilon_0 m^2} \times \varepsilon_{V,C} \int_{BZ} \frac{2dk}{(2\pi)^2} \frac{\left|a \times M_{V,C}(k)\right|^2}{E_C(k) - E_V(k)/\hbar} \times \frac{1}{\left[E_C(k) - E_V(k)\right]^2 \Big/ \hbar^2 - \omega^2} \quad (9)$$

$$\alpha(\omega) = \frac{2k\omega}{c} = \frac{2\pi k}{\lambda_0} \quad (10)$$

$$R(\omega) = \frac{(n-1)^2 + k^2}{(n+1)^2 + k^2} \quad (11)$$

where n is the refractive index, k is the extinction coefficient, ε_0 is the vacuum dielectric constant, λ_0 is the wavelength of light in a vacuum, C and V are the conduction band and valence band, respectively, BZ is the first Brillouin zone, K is the electron wave vector, **a** is the unit direction vector of the vector potential A, M_{VC} is the transition matrix element, ω is the angular frequency and $E_C(\omega)$ and $E_V(\omega)$ are the intrinsic energy levels of the conduction band and valence band, respectively.

An understanding of the electronic structures can be reached by investigating the optical spectra, which not only give information about the occupied and unoccupied states, but also about the features of the bands. Thus we investigated the optical properties of the $KPdCu(Se_2)(Se_3)$ and $RbPdCu(Se_2)(Se_3)$ compounds. The dielectric function connects the microscopic physical transitions between bands with the electronic structures of a solid, reflecting the band structure of the solid and providing information about its spectrum. In using $KPdCu(Se_2)(Se_3)$ and $RbPdCu(Se_2)(Se_3)$ as semiconductor materials, their spectra are generated by electronic transitions between energy levels and all the dielectric peaks can be explained using the calculated energy band structure and DOS. Fig. 5a and b show the spectra of the real and imaginary parts of the complex dielectric function *versus* the photon energy. As is clear from the above-mentioned calculation, there is no remarkable difference in the electronic structure of the spin-up and spin-down states, so the optical properties are discussed here using only the spin-up state. Our analysis of the $\varepsilon_2(\omega)$ spectrum (Fig. 5a) shows that the first critical point of the dielectric function occurs at 0.30 eV. This point is $Y_v - Y_c$, which gives the threshold for the optical transitions between the VBM and the CBM. This is known as the fundamental absorption edge. Beyond this threshold energy (the first critical point), the curve increases rapidly. This is because the number of points contributing towards $\varepsilon_2(\omega)$ increases abruptly. As the investigated compounds have a monoclinic symmetry, only three tensor components are needed to describe all the optical properties. These are: $\varepsilon_2^{xx}(\omega)$, $\varepsilon_2^{yy}(\omega)$ and $\varepsilon_2^{zz}(\omega)$. The main peak of the $\varepsilon_2^{xx}(\omega)$, $\varepsilon_2^{yy}(\omega)$ and $\varepsilon_2^{zz}(\omega)$ spectrum is at about 2.0 eV; there are also a second pronounced peak and three humps (Fig. 5a and b).

The real part of $\varepsilon_1(\omega)$ can be obtained using the Kramers–Kronig transformation. The results for the dispersive part of the dielectric function, $\varepsilon_1(\omega)$ for these compounds are shown in Fig. 5c and d. The main features in this spectrum are the peak around 1.8 eV, the rather steep decrease below 9.0 eV, after which $\varepsilon_1(\omega)$ becomes negative, and the minimum followed by a slow increase towards zero at high energies. In the energy range in which $\varepsilon_1(\omega)$ is negative, the electromagnetic wave is not

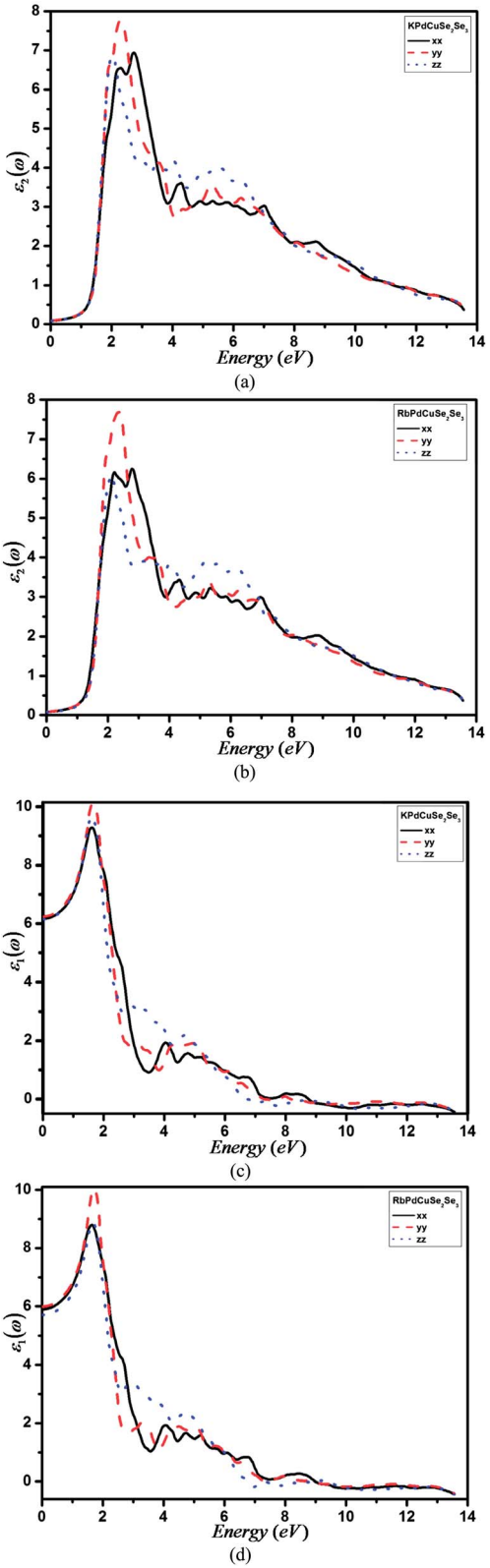

Fig. 5 Calculated imaginary $\varepsilon_2(\omega)$ and real $\varepsilon_1(\omega)$ parts of the dielectric tensor.

propagated. For the real dielectric function, the most important quantity is the zero frequency limit $\varepsilon_1(0)$, as this gives the static dielectric constant in the zero frequency limits, which has values of 6.168 (5.908), 6.240 (5.994) and 6.149 (5.718) for $\varepsilon_1^{xx}(0)$, $\varepsilon_1^{yy}(0)$ and $\varepsilon_1^{zz}(0)$ for KPdCu(Se_2)(Se_3) and (RbPdCu(Se_2)(Se_3)), respectively.

Fig. 6a–h show the energy loss function $L(\omega)$, reflectivity $R(\omega)$, refractivity $n(\omega)$ and absorption coefficient $I(\omega)$. The complex refractive index $[\tilde{n}(\omega) = n(\omega) + ik(\omega)]$ portrays the refraction and also the absorption of the compounds. It contains two parts: the real part, $n(\omega)$, is the refractive index second-order tensor, whereas the other part, $k(\omega)$, is the extinction tensor, which represents the loss of photon energy during propagation through the optical medium. The premeditated refractive indices for KPdCu(Se_2)(Se_3) and RbPdCu(Se_2)(Se_3) are illustrated in Fig. 6a and b. The calculated non-zero tensor components of the static refractive index $n^{xx}(0)$, $n^{yy}(0)$ and $n^{zz}(0)$ are 2.483, 2.498 and 2.479 for KPdCu(Se_2)(Se_3) and 2.430, 2.448 and 2.391 for KPdCu(Se_2)(Se_3), respectively. According to Penn's model,[36] $\varepsilon_1(0)$ relates to the band gap of the material and $\varepsilon_1(0)$ is directly related to $n(0)$ by the relation $n(\omega) = \sqrt{\varepsilon_1(0)}$. They are improved beyond the zero frequency limits, reaching their maximum values. After the maximum values they start to decrease and, with few oscillations, are greater than unity. In this region ($n < 1$) the phase velocity of the photons enhances, approaching the universal constant (C). In contrast, the group velocity is always less than C and, as a consequence, the relativity relations are not affected.[37] The spectrum moves towards lower energy when the cations are changed from K to Rb. This is in agreement with the decrease in the band gap. The absorption spectra of KPdCu(Se_2)(Se_3) and RbPdCu(Se_2)(Se_3) (Fig. 6c and d) shows that both these materials absorb radiation at 2.0 eV. The absorption spectra show an uppermost value of 13.6 eV, analogous to the minimum values of $\varepsilon_1(\omega)$ and $\varepsilon_2(\omega)$ shown in Fig. 5a–d.

The frequency dependent reflectivities $R^{xx}(\omega)$, $R^{yy}(\omega)$ and $R^{zz}(\omega)$ were calculated and are shown in Fig. 6e and f. The reflectivity spectra of the compounds originates from the zero energy which characterizes the static part of the reflectivity components $R^{zz}(0)$, $R^{yy}(0)$ and $R^{xx}(0)$. These values are equal to 0.173, 0.176 and 0.168 for KPdCu(Se_2)(Se_3) and 0.181, 0.183 and 0.180 for RbPdCu(Se_2)(Se_3). The energy loss function $L^{xx}(\omega)$, $L^{yy}(\omega)$ and $L^{zz}(\omega)$, as illustrated in Fig. 6g and h, is a key component in the evaluation of the usefulness of energy of the material due to very fast electrons. The sharp spectral peaks produced in $L^{xx}(\omega)$, $L^{yy}(\omega)$ and $L^{zz}(\omega)$ around 11.8 eV for KPdCu(Se_2)(Se_3) and at 12.0 eV for RbPdCu(Se_2)(Se_3) are due to the occurrence of plasmon excitations.[38] It is observed that the relative maximum in the energy loss function occurs with a good approximation at energies where the dielectric function $\varepsilon_1(\omega)$ crosses the zero.

3.5. Thermal properties

The main aim of this work was to determine the thermoelectric properties of APdCu(Se_2)(Se_3) (A = K and Rb) and their variation with temperature. It is essential to guesstimate the effective masses of the carriers in different electron and hole pockets to achieve this. We calculated the effective mass (electron, heavy hole and light hole) ratio of the carriers at the conduction and valence band edges by fitting the energy of the respective bands to a quadratic polynomial in the reciprocal lattice vector $\tilde{k}$ as discussed earlier. It is apparent that the bands are less dispersive in the KPdCu(Se_2)(Se_3) structure in almost all the high symmetry directions. This is why we aimed for a large effective mass to obtain a high thermo-power. The existence of high mobility carriers is essential in attaining a higher electrical conductivity. Thus there is an opportunity to gain a large figure of merit (ZT) factor in these compounds by having multiple pockets of carriers with both large and small effective masses, with the former leading to a large Seebeck coefficient (S) and the latter improving $\sigma(\tau)$.[39,40] It is encouraging to note that the electronic structure of the investigated compounds shows the existence of multiple carrier pockets with significantly dissimilar effective masses, thereby signifying that they may have good thermoelectric properties.

For the conductivity coefficient calculation, the relaxation time term τ should be treated as a constant. Fig. 7a and b show the calculated temperature-dependent electrical conductivities for the studied compounds as a function of the relaxation time, $\sigma(\tau)$, within the temperature range 300–800 K, which is given as the σ^{xx}, σ^{yy} and σ^{zz} components. It was found that the conductivity as a function of relaxation time is anisotropic. Assuming that the relaxation time τ is direction-independent, the values of the σ^{xx} and σ^{zz} components at 800 K are smaller than the value of the σ^{yy} component.

The σ^{xx}, σ^{yy} and σ^{zz} values increase rapidly with increasing temperature, confirming the semiconductor-like transportation and temperature-sensitive conduction; this is in good agreement with the calculated electronic band structure. The anisotropic nature should be enhanced at higher temperatures, as shown in Fig. 7a and b. Although there is anisotropy in σ^{xx}, σ^{yy} and σ^{zz} at 300 K, this anisotropy is much greater at higher temperatures. The maximum conductivity values as a function of relaxation time reach $6 \times 10^{18}\ \Omega^{-1}\ m^{-1}\ s^{-1}$, $1.72 \times 10^{18}\ \Omega^{-1}\ m^{-1}\ s^{-1}$ and $4.8 \times 10^{18}\ \Omega^{-1}\ m^{-1}\ s^{-1}$ within the σ^{xx}, σ^{yy} and σ^{zz} components, respectively, for KPdCu(Se_2)(Se_3). In the KPdCu(Se_2)(Se_3) compound the σ^{xx} and σ^{zz} components show weak anisotropy with increasing temperature up to 550 K; the anisotropy then increases with increasing temperature. The anisotropy between the σ^{xx} and σ^{zz} components is comparatively much smaller than that of σ^{xx} and σ^{zz} with the σ^{yy} component. As K is replaced by Rb, the conductivity in both compounds increases with increasing temperature. In RbPdCu(Se_2)(Se_3) there is isotropy between the σ^{xx} and σ^{zz} components over the whole temperature range, although the σ^{xx} and σ^{zz} components show considerable anisotropy with the σ^{yy} component. The maximum conductivity values for RbPdCu(Se_2)(Se_3) as a function of relaxation time reach $0.5 \times 10^{18}\ \Omega^{-1}\ m^{-1}\ s^{-1}$ for the σ^{xx} and σ^{zz} components and about $6.85 \times 10^{18}\ \Omega^{-1}\ m^{-1}\ s^{-1}$ for the σ^{yy} component. From the conductivity spectra of both compounds we concluded that KPdCu(Se_2)(Se_3) shows a greater increase in conductivity than KPdCu(Se_2)(Se_3).

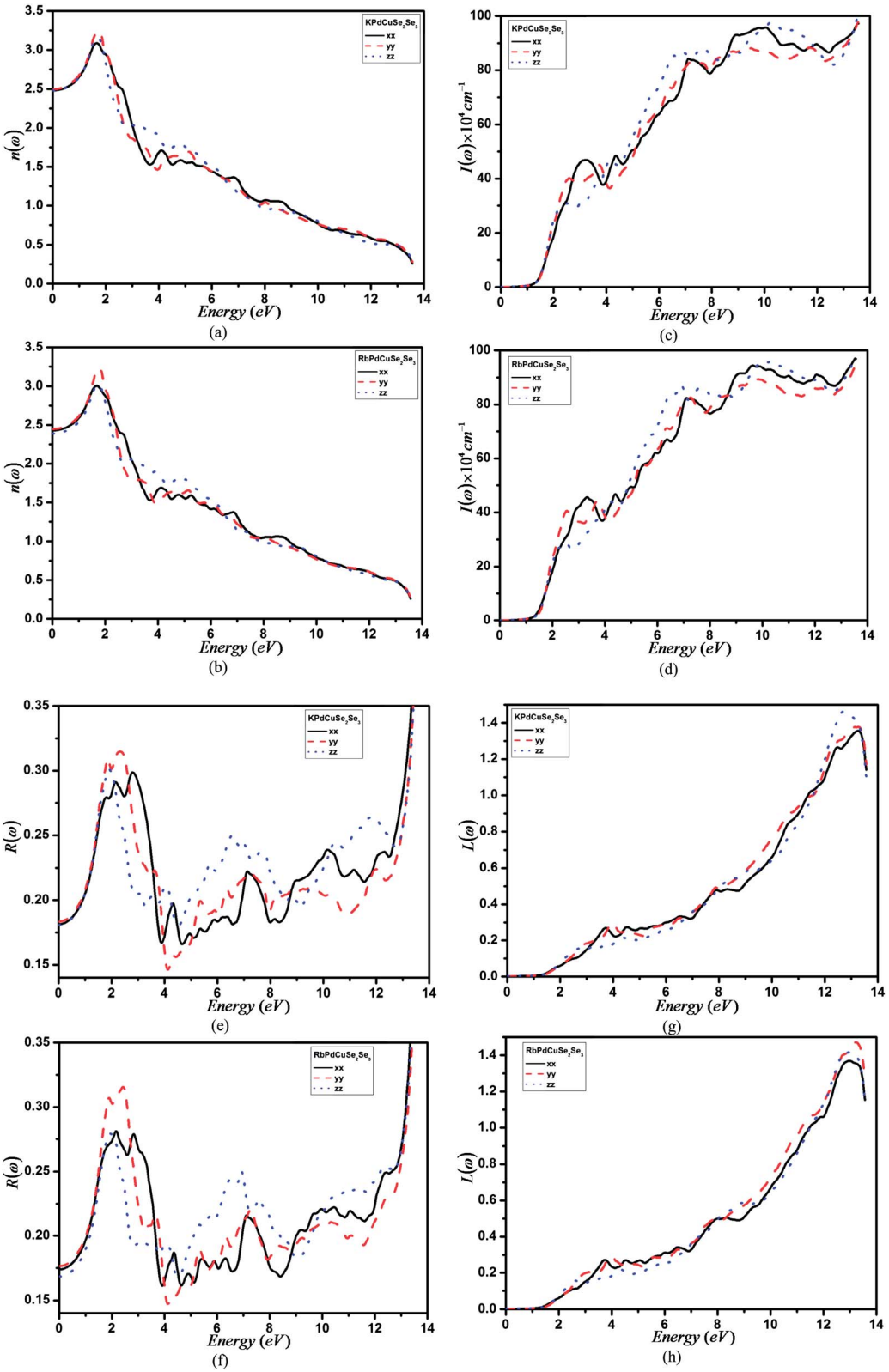

Fig. 6 Calculated refractivity $n(\omega)$, absorption coefficient $I(\omega)$, reflectivity $R(\omega)$ and energy-loss function spectrum $L(\omega)$.

Fig. 7c and d present the calculated temperature-dependent Seebeck coefficients, denoted as the S^{xx}, S^{yy} and S^{zz} components, for the $APdCu(Se_2)(Se_3)$ (A = K and Rb) compounds in the temperature range 300–800 K. It was found that the Seebeck coefficient as a function of temperature is also anisotropic; the S^{xx}, S^{yy} and S^{zz} components show reverse behaviors with respect

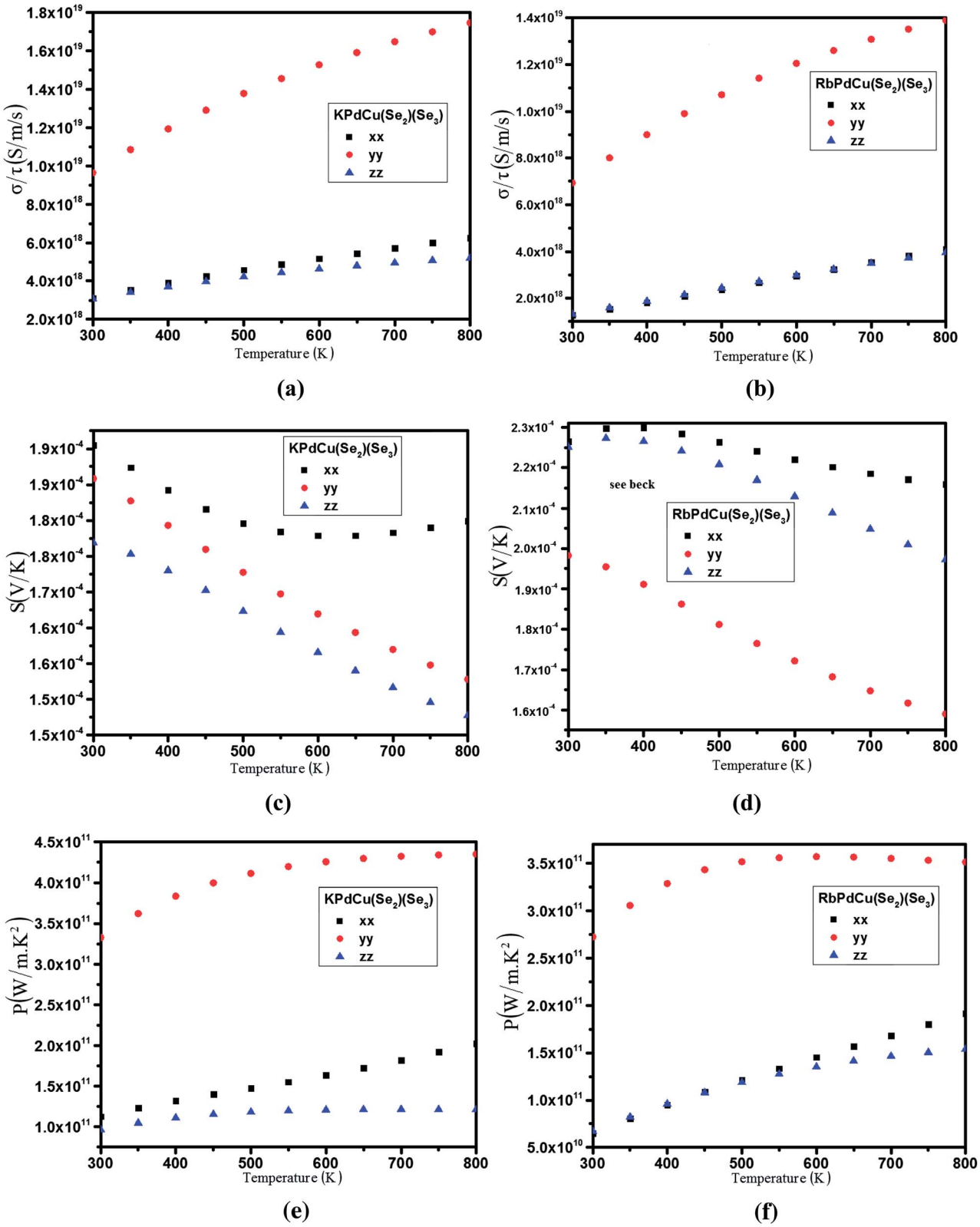

Fig. 7 Calculated thermoelectric properties: electrical conductivity, Seebeck coefficients and power factor.

to the conductivity as a function of temperature. For example, the S value within 'S^{yy}' component is larger than that within the S^{xx} and S^{zz} components and the anisotropic nature remains the same in the higher temperature region. The values of the S^{xx}, S^{yy} and S^{zz} components show positive temperature dependence. It was also observed that the values of S^{xx}, S^{yy} and S^{zz} tends to be

completely saturated in the high temperature region, reaching 1.83 (2.16) $\times 10^{-4}$, 1.57 (1.97) $\times 10^{-4}$ and 1.55 (1.59) $\times 10^{-4}$ for the S^{xx}, S^{yy} and S^{zz} components, respectively, for KPdCu(Se$_2$)(Se$_3$) and (RbPdCu(Se$_2$)(Se$_3$)) at 800 K. From a consideration of the conductivity dependence as a function of temperature, the electrical performance should be enhanced with increasing temperature.

As we replace K by Rb, the decrease in the Seebeck coefficient for both compounds is the same with increasing temperature. The three components show considerable anisotropy with increasing temperature in both compounds. If we look at the spectra, with increasing temperature the S^{xx}, S^{yy} and S^{zz} components decrease, but the S^{xx} component shows a different behavior to the S^{yy} and S^{zz} components. The S^{xx} component decreases to 600 K, is at equilibrium at 650 K, and then starts to increase with increasing temperature. At low temperatures, RbPdCu(Se$_2$)(Se$_3$) has a larger Seebeck coefficient than KPdCu(Se$_2$)(Se$_3$).

Fig. 7e and f show the calculated temperature-dependent power factor (PF) as a function of relaxation time in the temperature interval 300–800 K, denoted as P^{xx}, P^{yy} and P^{zz}. The PF value within the P^{xx} and P^{zz} components at 800 K is smaller than the value of the P^{yy} component, assuming that the relaxation time τ is independent of direction. The PF values increase rapidly with increasing temperature, confirming that the electrical performance is sensitive to temperature. The anisotropic nature is enhanced at higher temperatures (Fig. 7e and f). In KPdCu(Se$_2$)(Se$_3$) the P^{xx} and P^{zz} components show weak anisotropy at low temperatures, but the anisotropy increases with increasing temperature; the anisotropy between these two components is comparatively very much smaller than that along the P^{yy} component. In contrast, in RbPdCu(Se$_2$)(Se$_3$) the P^{xx} and P^{zz} components show isotropy up to 550 K, which increases with increasing temperature; both the P^{xx} and P^{zz} components show considerable anisotropy with the P^{yy} component. We emphasize that KPdCu(Se$_2$)(Se$_3$) shows a greater PF value than KPdCu(Se$_2$)(Se$_3$). The maximum PF values as a function of relaxation time are 4.3 (3.5) $\times 10^{11}$, 2.0 (1.57) $\times 10^{11}$ and 1.2 (1.5) $\times 10^{11}$ W m^{-1} K^{-2} s^{-1} for the P^{xx}, P^{yy} and P^{zz} components, respectively, for KPdCu(Se$_2$)(Se$_3$) and RbPdCu(Se$_2$)(Se$_3$). From the analysis of both compounds, we concluded that they both possess good thermoelectric properties at high temperatures, but that KPdCu(Se$_2$)(Se$_3$) shows much better thermoelectric behavior than RbPdCu(Se$_2$)(Se$_3$); this is attributed to the fact that at higher temperatures KPdCu(Se$_2$)(Se$_3$) shows a better PF value than RbPdCu(Se$_2$)(Se$_3$).

4. Conclusions

In summary, the electronic band structure, optical properties and electrical transport coefficients of APdCu(Se$_2$)(Se$_3$) (A = K and Rb), a new quaternary copper palladium polyselenide, were studied. From this study of the electronic band structure, we concluded that the valence band maximum and conduction band minimum are positioned at the Y point, resulting in a direct energy band gap of about 1.258/1.275 eV. From the PDOS we also concluded that at an energy of −5.0 eV, the Pd-s state strongly hybridizes with the Se-p state. Near the Fermi level, the Se-p state hybridizes with the Cu-p state, and at the low conduction band the Pd-s state forms a strong hybridization with the Cu-s state. We have also calculated the electronic charge density in the (010) plane. It can be seen that the Pd–Se and Cu–Se atoms form weak covalent bonds and strong ionicity, whereas the K/Pd atoms show pure ionic bonding. We have also calculated the effective mass ratio of the electrons, heavy holes and light holes. The calculated effective mass ratio for the electron, heavy holes and light holes for KPdCu(Se$_2$)(Se$_3$)/(RbPdCu(Se$_2$)(Se$_3$)) are 0.0332/(0.0225), 0.1350/(0.0202) and 0.1858/(0.0198), respectively. The real and imaginary parts of the dielectric function and hence the optical constants, such as the refractive index and extinction coefficient, were calculated and discussed in detail. From the absorption spectrum we concluded that both KPdCu(Se$_2$)(Se$_3$) and RbPdCu(Se$_2$)(Se$_3$) begin to absorb radiation at around 1.8–2.0 eV. The absorption spectra show an uppermost value at 13.6 eV, analogous to the minimum value of $\varepsilon_1(\omega)$ and $\varepsilon_2(\omega)$. The Seebeck coefficient, together with the conductivity and the PF as a function of relaxation time were calculated systematically. The calculated conductivity and Seebeck coefficient confirm the anisotropic nature and the semiconductor transport behavior of the compounds. The calculated PF as a function of relaxation time increases rapidly with increasing temperature. The maximum PF values as a function of relaxation time reach 4.3 (3.5) $\times 10^{11}$, 2.0 (1.57) $\times 10^{11}$ and 1.2 (1.5) $\times 10^{11}$ W m^{-1} K^{-2} s^{-1} for the P^{xx}, P^{yy} and P^{zz} components, respectively, for KPdCu(Se$_2$)(Se$_3$) and RbPdCu(Se$_2$)(Se$_3$) at 800 K. The present calculation of the thermoelectrical behavior of APdCu(Se$_2$)(Se$_3$) (A = K and Rb) for the PF suggests that both compounds show good thermoelectric properties at high temperatures.

Acknowledgements

The work was developed within the CENTEM Project, Reg. no. CZ.1.05/2.1.00/03.0088, co-funded by the ERDF as part of the Ministry of Education, Youth and Sports OP RDI Programme.

References

1 (*a*) H. Eckert, *Angew. Chem., Int. Ed. Engl.*, 1989, **28**, 1723; (*b*) Y. Wang, N. Herron, W. Mahler and A. Suna, *J. Opt. Soc. Am. B*, 1989, **6**, 808; (*c*) R. Chung, T. Hogan, P. Brazis, M. Rocci-Lane, C. Kannewurf, M. Bastea, C. Uher and M. G. Kanatzidis, *Science*, 2000, **287**, 1024.
2 W. S. Sheldrick and M. Wachhold, *Coord. Chem. Rev.*, 1998, **176**, 211.
3 M. G. Kanatzidis and A. C. Sutorik, *Prog. Inorg. Chem.*, 1995, **43**, 15.
4 M. G. Kanatzidis, *Curr. Opin. Solid State Mater. Sci.*, 1997, **2**, 139.
5 M. G. Kanatzidis and B. K. Das, *Comments Inorg. Chem.*, 1999, **21**, 29.
6 W. S. Sheldrick and M. Wachhold, *Angew. Chem., Int. Ed. Engl.*, 1997, **36**, 206.
7 G. Kräuter and K. Dehnicke, *Chem.-Ztg.*, 1990, **114**, 7–9.

8 K.-W. Kim and M. G. Kanatzidis, *J. Am. Chem. Soc.*, 1998, **120**, 8124–8135.
9 M. Wachhold and M. G. Kanatzidis, *J. Am. Chem. Soc.*, 1999, **121**, 4189–4195.
10 K.-W. Kim and M. G. Kanatzidis, *J. Am. Chem. Soc.*, 1992, **114**, 4878.
11 J. Li, Z. Chen, R.-J. Wang and J. Y. J. Lu, *Solid State Chem.*, 1998, **140**, 149.
12 J. Llanos, C. Contreras-Ortega, C. Mujica, H. G. von Schnering and K. Peters, *Mater. Res. Bull.*, 1993, **28**, 39–44.
13 C. Mujica, J. Paez and J. Llanos, *Mater. Res. Bull.*, 1994, **29**, 263–268.
14 J. Li, H.-Y. Guo, R. A. Yglesias and T. Emge, *Chem. Mater.*, 1995, **7**, 599–601.
15 J. Llanos, C. Contreras-Ortega, J. Paez, M. Guzman and C. Mujica, *J. Alloys Compd.*, 1993, **201**, 103–104.
16 J. Llanos, P. Valenzuela, C. Mujica, A. Buljan and R. Ramirez, *J. Solid State Chem.*, 1996, **122**, 31–35.
17 X. Chen, K. J. Dilks, X. Huang and J. Li, *Inorg. Chem.*, 2003, **42**, 3723–3727.
18 P. Guss, M. E. Foster, B. M. Wong, F. Patrick Doty, K. Shah, M. R. Squillante, U. Shirwadkar, R. Hawrami, J. Tower and D. Yuan, *J. Appl. Phys.*, 2014, **115**, 034908.
19 V. I. Anisimov, F. Aryasetiawan and A. I. Lichtensteinet, *J. Phys.: Condens. Matter*, 1997, **9**, 767.
20 J. P. Perdew, B. Kieron and E. Matthias, *Phys. Rev. Lett.*, 1996, **77**, 3865–3868.
21 P. Hohenberg and W. Kohn, *Phys. Rev. B: Condens. Matter Mater. Phys.*, 1996, **136**, B864.
22 W. Kohn and L. J. Shom, *Phys. Rev.*, 1965, **140**, A1133.
23 P. Blaha, K. Schwarz and J. Luitz, *WIEN97: A full potential linearized augmented plane wave package for calculating crystal properties*, ISBN: 3-9501031-0-4, Karlheinz Schwarz. Techn. Universit at Wien, Austria, 1991.
24 C. Loschen, J. Carrasco, K. M. Neyman and F. Illas, *Phys.Rev. B: Condens. Matter Mater. Phys.*, 2007, **75**, 035115.
25 J. C. Li, C. L. Wang, M. X. Wang, H. Peng, R. Z. Zhang, M. L. Zhao, J. Liu, J. L. Zhang and L. M. Mei, *J. Appl. Phys.*, 2009, **105**, 043503.
26 A. Popescu, L. M. Woods, J. Martin and G. S. Nolas, *Phys. Rev. B: Condens. Matter Mater. Phys.*, 2009, **79**, 205302.
27 M. Zebarjadi, K. Esfarjani, M. S. Dresselhaus, Z. F. Ren and G. Chen, *Energy Environ. Sci.*, 2012, **5**, 5147.
28 L. Bertini and C. Gatti, *J. Chem. Phys*, 2004, **121**, 8983.
29 Y. Wang, X. Chen, T. Cui, Y. Niu, Y. Wang, M. Wang, Y. Ma and G. Zou, *Phys. Rev. B: Condens. Matter Mater. Phys.*, 2007, **76**, 155127.
30 L. Lykke, B. B. Iversen and G. K. H. Madsen, *Phys. Rev. B: Condens. Matter Mater. Phys.*, 2007, **73**, 195121.
31 D. B. Sirdeshmukh, L. Sirdeshmukh and K. G. Subhadra, *Alkali Halides: A Handbook of Physical Properties*, ed. R. Hull, R. M. Osgood Jr, H. Sakaki and A. Zunger, Springer-Verlag, Berlin, 2001, pp. 249, 251.
32 G. K. H. Madsen and D. J. Singh, *Comput. Phys. Commun.*, 2006, **175**, 67.
33 R. C. Fang, *Spectroscopy of Solid*, University of Science and Technology Press, Hefei, China, 2001, pp. 71–75.
34 X. C. Sheng, *Spectrum and Optical Property of Semiconductor*, Science Press, Beijing, 2002, pp. 76–94.
35 Q. Chen, Q. Xie and W. J. Yan, *Sci. China, Ser. G: Phys., Mech. Astron.*, 2008, **38**(7), 825–833.
36 D. R. Penn, *Phys. Rev. B: Solid State*, 1962, **128**, 2093–2097.
37 M. Fox, *Optical Properties of Solids*, Oxford University Press, 2001.
38 L. Marton, *Rev. Mod. Phys.*, 1956, **28**, 172–184.
39 D. Parker and D. J. Singh, *Phys. Rev. B: Condens. Matter Mater. Phys.*, 2012, **85**, 125209.
40 D. J. Singh and I. I. Mazin, *Phys. Rev. B: Condens. Matter Mater. Phys.*, 1997, **56**, R1650–R1653.